Metahouse: Noise-Insulating Chamber Based on Periodic Structures

Mariia Krasikova,* Sergey Krasikov, Anton Melnikov,* Yuri Baloshin, Steffen Marburg, David A. Powell, and Andrey Bogdanov

In Memoriam to Yuri Baloshin (1940–2022)

Noise pollution remains a challenging problem requiring the development of novel systems for noise insulation. Extensive work in the field of acoustic metamaterials has led to various ventilated structures which, however, are usually demonstrated for rather narrow regions of the audible spectrum. In this work, the idea of metamaterial-based systems is further extended, developing the concept of a metahouse chamber representing a ventilated structure for multiple band noise insulation. Broad stop-bands originate from strong coupling between pairs of Helmholtz resonators constituting the structure. The averaged transmission −18.6 dB are demonstrated numerically and experimentally within the spectral range from 1500 to 16 500 Hz. The sparseness of the structure together with the possibility to use optically transparent materials suggest that the chamber may be also characterized by partial optical transparency depending on the mutual position of structural elements. The obtained results are promising for development of novel noise-insulating structures advancing urban science.

1. Introduction

Acoustic metamaterials and phononic crystals have been subjects of keen scientific interest for a couple of decades as they

M. Krasikova, S. Krasikov, Y. Baloshin,[†] A. Bogdanov
School of Physics and Engineering
ITMO University
St. Petersburg 197101, Russia
E-mail: mariia.krasikova@metalab.ifmo.ru

A. Melnikov, S. Marburg
Chair of Vibroacoustics of Vehicles and Machines
Technical University of Munich
Garching b., 85748 München, Germany
E-mail: anton.melnikov@ipms.fraunhofer.de

D. A. Powell
School of Engineering and Information Technology
University of New South Wales
Northcott Drive, Canberra, Australian Capital Territory 2600, Australia

A. Bogdanov
Harbin Engineering University
Harbin, Heilongjiang 150001, P. R. China

[†]Deceased, July 4, 2022

provide novel routes toward efficient control of acoustic fields.[1–4] In addition to the realization of negative refractive index,[5] superlenses,[6,7] holograms,[8] and acoustic cloaks,[9] recent advances include the development of nonreciprocal systems,[10] topological insulators,[11,12] nonlinear,[13] tunable,[14] coding,[15] and programmable metasurfaces.[16] Acoustic metasurfaces were also explored as potential platforms for analog computing[17] and advances in computer science and artificial intelligence boost design procedures to achieve desired properties of metamaterials and metasurfaces.[18–21] Metamaterials can be also used as a platform to explore analogies of the quantum concepts, such as Hall effect,[22,23] spin properties,[24–27] skyrmions,[28] and twistronics.[29]
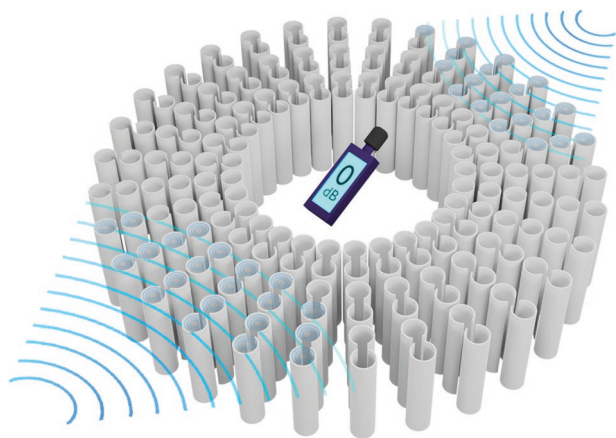
One of the developing branches in the field of acoustic metamaterials is dedicated to the realization of novel noise-insulating systems.[30] Increasing noise pollution in urban areas is one of the endangering trends affecting global health and the ecological environment.[31–35] Solution of this problem requires the development of new methods and materials allowing broadband passive noise insulation. Conventionally used systems are typically represented by bulky structures imposing harsh engineering restrictions on buildings and constructions.[36] The frequency range of noise mitigation has to be compromised with mass and volume of the used materials. Moreover, some crucial properties like ventilation or optical transparency are usually incompatible with such systems.

Instead of the conventional mass–density law, reflection and attenuation of sound in metamaterials relies mostly on the periodicity and shape of the structural elements rather than their material properties. One of the important options enabled by metamaterials is the possibility to implement structures allowing air flow.[37–41] A variety of designs includes perforated membranes,[42,43] space coiling structures,[44–48] and metacages[49–51] have been presented. Nevertheless, despite the plethora of achievable physical effects, acoustic metamaterials rarely find real-life applications. These structures usually have complicated designs and a narrow operating range.

In this paper, we propose a noise-insulating ventilated metahouse chamber allowing access of light into the inner area. The chamber is designed to be simple for manufacturing and assembling. At the same time, the requirements for materials

Figure 1. Metahouse concept. The Helmholtz resonators are shown with gray only for clarity and can be made of transparent materials. The inner space of the developed chamber is protected from acoustic noise within a broad audible spectral range. At the same time, the structure is ventilated and optically transparent, depending solely on the distance between the structural elements and their size, which also determine the spectral range of blocked noise.

$$f_{\Gamma X} = f_{\Gamma X}^{(1)} + f_{\Gamma X}^{(2)} + \ldots$$

Figure 2. Design of the unit cell. a) Illustration of the considered unit cell consisting of two locally coupled Helmholtz resonators. Width of the unit cell is a_x and the height is a_y. The resonators are characterized by the inner radius r and the outer radius R. Slit width w and distance between the resonators d are tuning parameters. The resonators are rotated around their out-of-plane axes by the angles θ_1 and θ_2. Dashed red lines indicate reflection symmetry axes of the cell. b) The corresponding reciprocal unit cell. c) Arbitrary band diagram representing labeling of individual ΓX band-gaps used for calculation of the integral width of ΓX band-gaps $f_{\Gamma X}$.
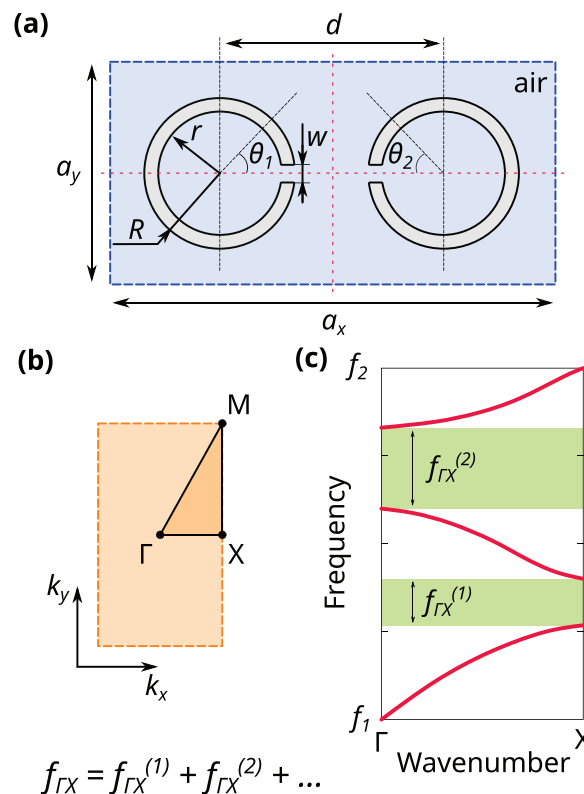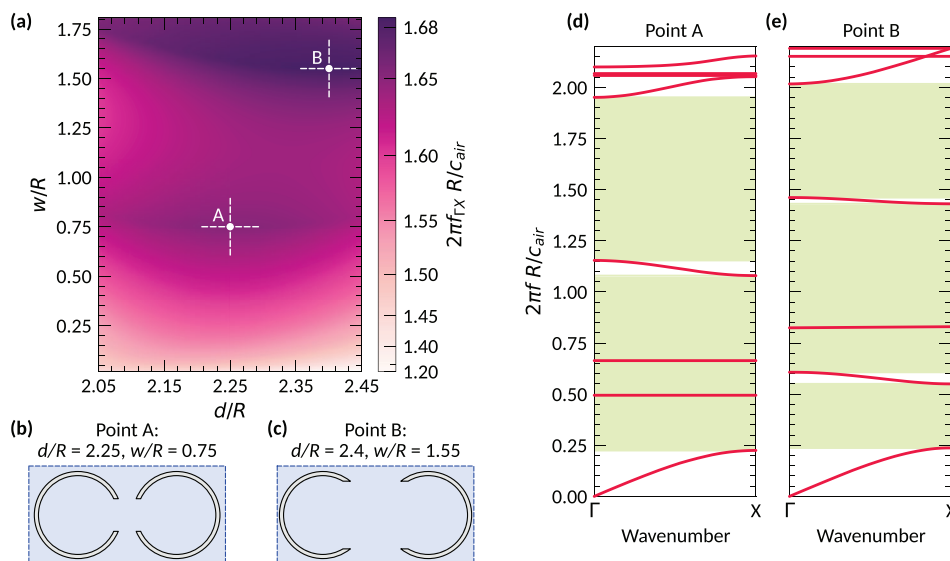
are easily met and the structure can be made of ecologically friendly and optically transparent materials. The chamber is based on coupled Helmholtz resonators with a C-shaped cross-section and exploits band-gap formation as the main mechanism for sound insulation. The artistic illustration of the concept is presented in **Figure 1**. It is proposed that such structures may be incorporated into urban parks and green zones to create noise-free relaxation zones for visitors. For this particular practical application the main engineering requirement is to have as large range of noise mitigation as it is possible. At the same time, there are no strict limitations on the thickness of the structure which allows to exploit properties of a metamaterial as well as a phononic crystal to achieve multiple stop-bands. In this sense our goal is different from the development of ultra-thin structures presented in literature.[38,51–53] Instead, we focus on the sparseness together with a number and width of stop-bands as these are the properties which are most desired for the mentioned applications. Under the sparseness we imply a low filling factor and large distance between the structural elements.

We start by designing a 2D metamaterial-based periodic structure and tuning its parameters for maximization of the integral width of band-gaps in the audible spectral range. Then, we perform an experimental demonstration of stop-bands corresponding to band-gaps of the infinite system. Finally, we provide an experimental demonstration of a finite-size prototype of the metahouse chamber. All experimental results are verified by numerical simulations.

2. Results

2.1. Design of a Unit Cell

The chosen unit cell consists of two coupled Helmholtz resonators with a C-shaped cross-section, as shown in **Figure 2**a.

Such resonators can be 3D printed or easily manufactured via simple mechanical processing of commercially available polymer pipes. Similar geometries were already considered for noise mitigation purposes[50,54,55] and we have just utilized the fact that local coupling between the resonators may increase the integral width of band gaps.[56] In this paper we consider only ΓX band-gaps since the implemented experimental realization of the semi-infinite structure implies that the incident plane wave has only k_x component. By tuning of geometrical parameters, we have optimized the system to further increase the integral width of band-gaps $f_{\Gamma X}$ defined as the sum of the widths of individual band-gaps (see Figure 2b,c)

$$f_{\Gamma X} = \sum f_{\Gamma X}^{(i)} \tag{1}$$

where i indicates the band-gap number and subscript ΓX indicates that the considered band-gaps lie within the ΓX interval of the Brillouin zone (see Figure 2b,c). Here it should be noted that summation is performed over the band-gaps within the considered frequency range. For simplicity, we have considered a 2D geometry assuming that the resonators are infinite in the direction perpendicular to the surface of the cross-section.

ADVANCED
SCIENCE NEWS
www.advancedsciencenews.com

ADVANCED
MATERIALS
TECHNOLOGIES
www.advmattechnol.de

Figure 3. Band structure and optimization. a) Integral width of band-gaps as a function of slit width w and distance between the resonators d. Points A and B indicate two local maxima of the function $f_{\Gamma X}$, occurring near the points with $w/R = 0.75$, $d/R = 2.25$, and $w/R = 1.55$, $d/R = 2.4$, respectively. The corresponding unit cells are shown in panels (b) and (c). Note that the map is rescaled using a power-law relationship to provide better visualization. Band diagrams for the structures with such configurations are demonstrated in panels (d) and (e). Shaded green areas indicate the ΓX band-gaps.

Since the system is scalable, for the tuning procedure we have normalized all geometric parameters to the outer radius of the resonators R. The size of the unit cell is fixed at values of $a_x/R = 4.5$ and $a_y/R = 2.25$. The inner radius of the resonators r is fixed as $r/R = 0.905$. The distance between the centers of resonators d as well as the width of slits w are varied as parameters directly affecting the local coupling. The frequencies are also normalized by R/c_{air}, where $c_{air} = 343\,ms^{-1}$ is the speed of sound in air.

The colormap shown in **Figure 3**a demonstrates the integral width of ΓX band-gaps $f_{\Gamma X}$ as a function of w and d. Clearly, the presence of finite-size slits results in the increase of $f_{\Gamma X}$. At the same time, the dependence is nonlinear and there are two local maxima corresponding to the points with $d/R = 2.25$, $w/R = 0.75$ (point A, see Figure 3b) and $d/R = 2.4$, $w/R = 1.55$ (point B, see Figure 3c). The corresponding band structures demonstrating large ΓX band-gaps are shown in Figure 3d,e, respectively. It is also important to note that within the considered frequency range the structure may possess the features of a metamaterial as well as a phononic crystal. So there may be several mechanisms of band-gap formation involved.
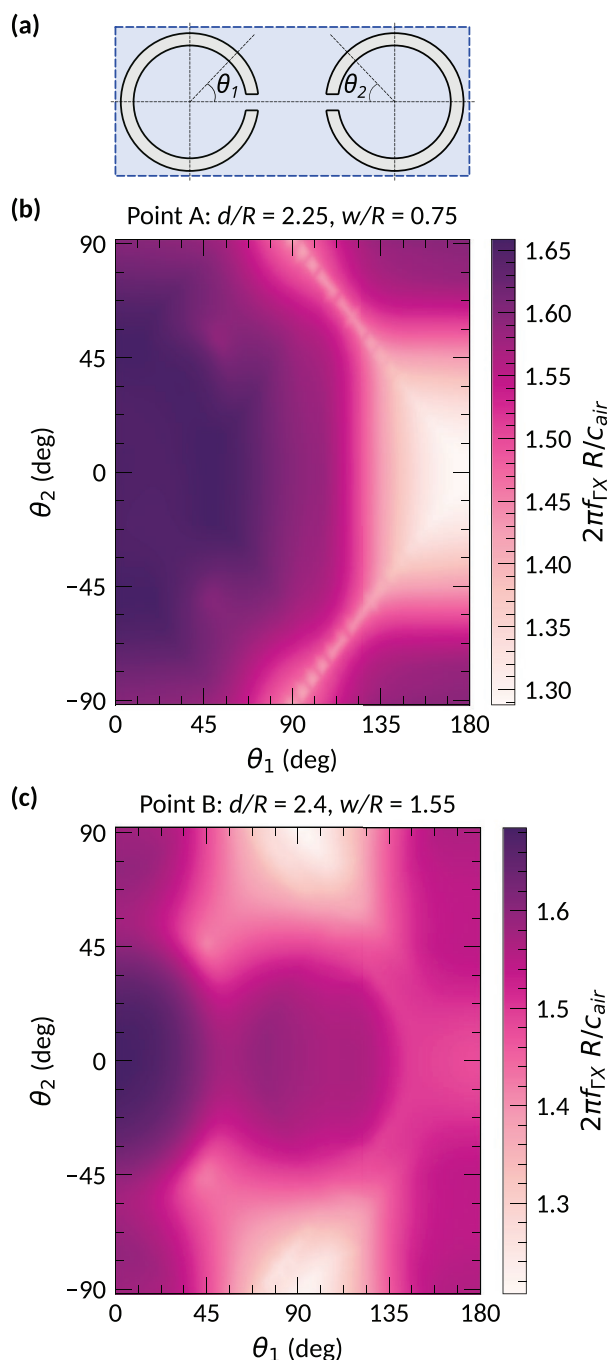
Following the adjustment of slit width and distance between the resonators, we analyze the effect of the resonators' rotation on the integral width of band-gaps. **Figure 4** shows the integral width of band-gaps calculated for the range of rotational angles θ_1 and θ_2 (see Figure 4a). Rotation of the resonators results in a pronounced decrease of $f_{\Gamma X}$ in the vicinity of the point $\theta_1 = 0°$, $\theta_2 = 180°$, corresponding to the case of CC-like geometry. Such a reduction of the integral width of band-gaps is associated with the decrease of local coupling strength[56] which in the case of CC-like geometry is weak. In the next section we demonstrate that the proposed geometry is indeed characterized by much stronger local coupling allowing an increase of the integral width of band gaps by nearly 30% compared to the CC-like geometry. Considering point A, for the CC-like geometry $f_{\Gamma X}$

is reduced by more than 20% compared to the optimal case with $\theta_1 = \theta_2 = 0°$ (see Figure 4b). Similarly, for point B the corresponding reduction is $\approx 15\%$ (see Figure 4c), however, there are configurations which are less beneficial. Figure 4 also demonstrates the robustness of the considered system against rotations of the resonators. Indeed, the calculations indicate that rotation within $\approx 15°$ has little effect on the value of $f_{\Gamma X}$. This robustness is important for practical realization of the proposed structure since it relaxes the required tolerances for mounting.

2.2. Coupled Helmholtz Resonators

Here we verify the strong local coupling between the Helmholtz resonators, which is the key mechanism for achieving multiple band noise insulation. We consider a pair of the resonators in free space and calculate the pressure inside one of them, assuming that the incident wave with the amplitude $p_0 = 1\,Pa$ propagates along the x-axis (see **Figure 5**a,d). The resulting spectra are shown in Figure 5b,e. The splitting of the Helmholtz resonance decreasing with the increase of the distance between the resonators is the manifestation of the coupling between the resonators. For the case of the considered geometry (Figure 5d), the splitting is much larger than for the CC-like one (Figure 5a). In addition, the field distribution in the proposed geometry is fundamentally different from the CC-like geometry since it has additional mirror symmetry with respect to the y-axis. Hence, the split Helmholtz resonance occurs as in-phase and out-of-phase excitation of the resonators characterized by symmetric and anti-symmetric field distributions, respectively (see Figure 5c,f).

In the case of an infinite array, the local coupling results in a pronounced increase of the integral width of band-gaps.[56] **Figure 6** demonstrates the difference between the band structures for the infinite arrays of resonators with zero slits (which

**ADVANCED
SCIENCE NEWS**

www.advancedsciencenews.com

**ADVANCED
MATERIALS
TECHNOLOGIES**

www.advmattechnol.de

(a)

(b)

Point A: $d/R = 2.25$, $w/R = 0.75$

(c)

Point B: $d/R = 2.4$, $w/R = 1.55$

Figure 4. Rotation of the resonators. a) The definition of the rotational angles θ_1 and θ_2. The strongly coupled geometry is characterized by $\theta_1 = \theta_2 = 0°$ while the case of the CC-like geometry corresponds to $\theta_1 = 0°$, $\theta_2 = 180°$. Colormaps show the integral width of band-gaps as a function of the rotational angles with the resonators characterized by b) $w/R = 0.75$, $d/R = 2.25$ and c) $w/R = 1.55$, $d/R = 2.4$. These parameters correspond to the points labeled as A and B, respectively in Figure 3.

are just circular pipes), CC-like geometry and strongly coupled resonators. Indeed, the introduction of slits into the pipes results in the formation of an additional band (see Figure 6b) as well as the additional band-gap, as a consequence. Further, enhancement of the local coupling leads to the formation of two more
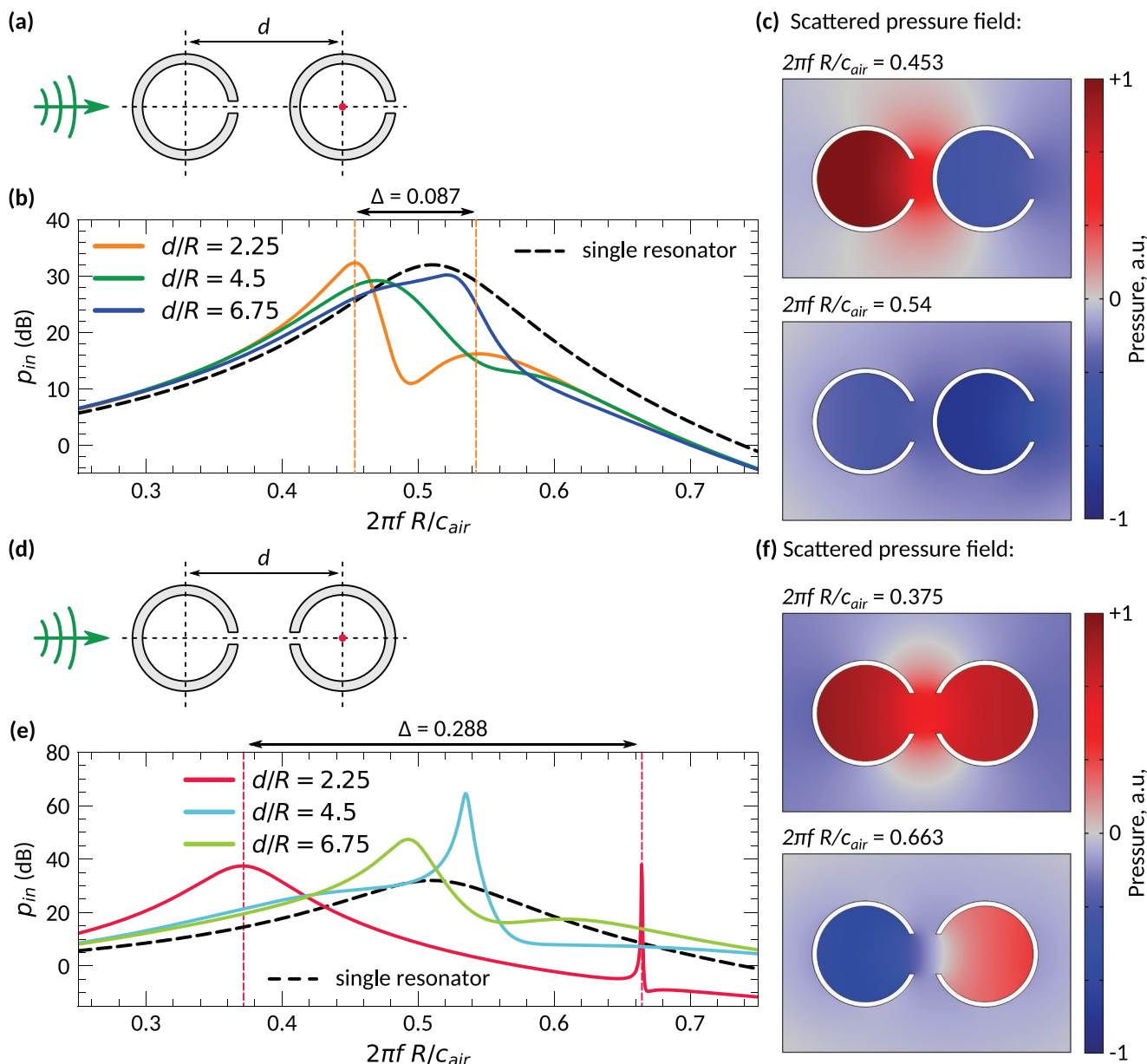
ΓX band-gaps. In this case, the out-of-phase excitation of the Helmholtz resonance corresponds to the flat band, indicating strong localization of the field inside the resonators as well as the absence of coupling between the neighboring pairs. In turn, the other mode, which is flat only within the ΓX interval, is associated with the in-phase excitation of the Helmholtz resonance.

To trace the evolution of the band structure caused by the introduction of the slit, and the consequent enhancement of local coupling, we consider field distributions within the unit cells at the Γ point. For the structure made of pipes there are two modes with zero frequency. One of them, labeled as a1-1 in Figure 6d, is a structural resonance, typical for periodic structures. This mode is present in both other band diagrams (Figure 6 b1,c1). Another mode, labeled as a1-2, is the flat band with zero frequency corresponding to the eigenmode of a Helmholtz resonator with no slit. As soon as the slit is introduced, this band deforms and shifts to the higher frequencies. Hence, the mode a1-2 of pipe arrays can be associated with the mode b2, which is a Helmholtz resonance of the CC-like structure. When the coupling is enhanced, this mode splits into two bands (Figure 6 c2,c3). In this case, the field distribution within a single unit cell of the periodic structure is similar to that observed for a single pair of resonators presented in Figure 5f. The anti-symmetric mode, labeled c3 is perfectly localized between the resonators, meaning that there is no coupling between neighboring pairs, which is the reason why the corresponding band is flat. There is an additional mode c4, which may be considered as the additional structural resonance resulting from the deformation of the unit cell.

There are also other modes with a flat spectrum, which are degenerate. For the case of pipes without slits, these modes are labeled as a2-1 and a2-2. When the slit is introduced, the degeneracy lifts due to the interaction, but a mode with similar field distribution remains in the system. Then, the structure with the strong coupling is characterized by two similar nearly-degenerate modes (c6-1 and c6-2). Finally, mode c5 is a structural resonance, such that similar resonances are present in all of the considered structures, but at higher frequencies. It also should be noted that despite the increasing width of the slit discussed in the previous section, dispersion of some modes remains flat manifesting weak interaction between the unit cells. The reason of this weak coupling can be understood from the symmetry of the modes and its profiles shown in Figure 6d.

2.3. Experimental Verification of Stop-Bands

To experimentally verify the presence of wide band-gaps, we consider a configuration of the structure corresponding to the point A in Figure 3. We imitate the semi-infinite structure, such that it is finite along one axis and infinite along the two other ones (see Experimental Section for details). The samples fabricated via 3D printing are shown in **Figure 7**a while the schematic view and photograph of the setup are shown in Figure 7b,c, respectively. Note that of instead the complete resonators we consider their halves utilizing the symmetry of the field distribution within the unit cell, as discussed in the Experimental Section. The measurements are performed for the unit cell characterized by $a_x = 240\,\text{mm}$ and $a_y = 120\,\text{mm}$ such that

ADVANCED
SCIENCE NEWS
www.advancedsciencenews.com

ADVANCED
MATERIALS
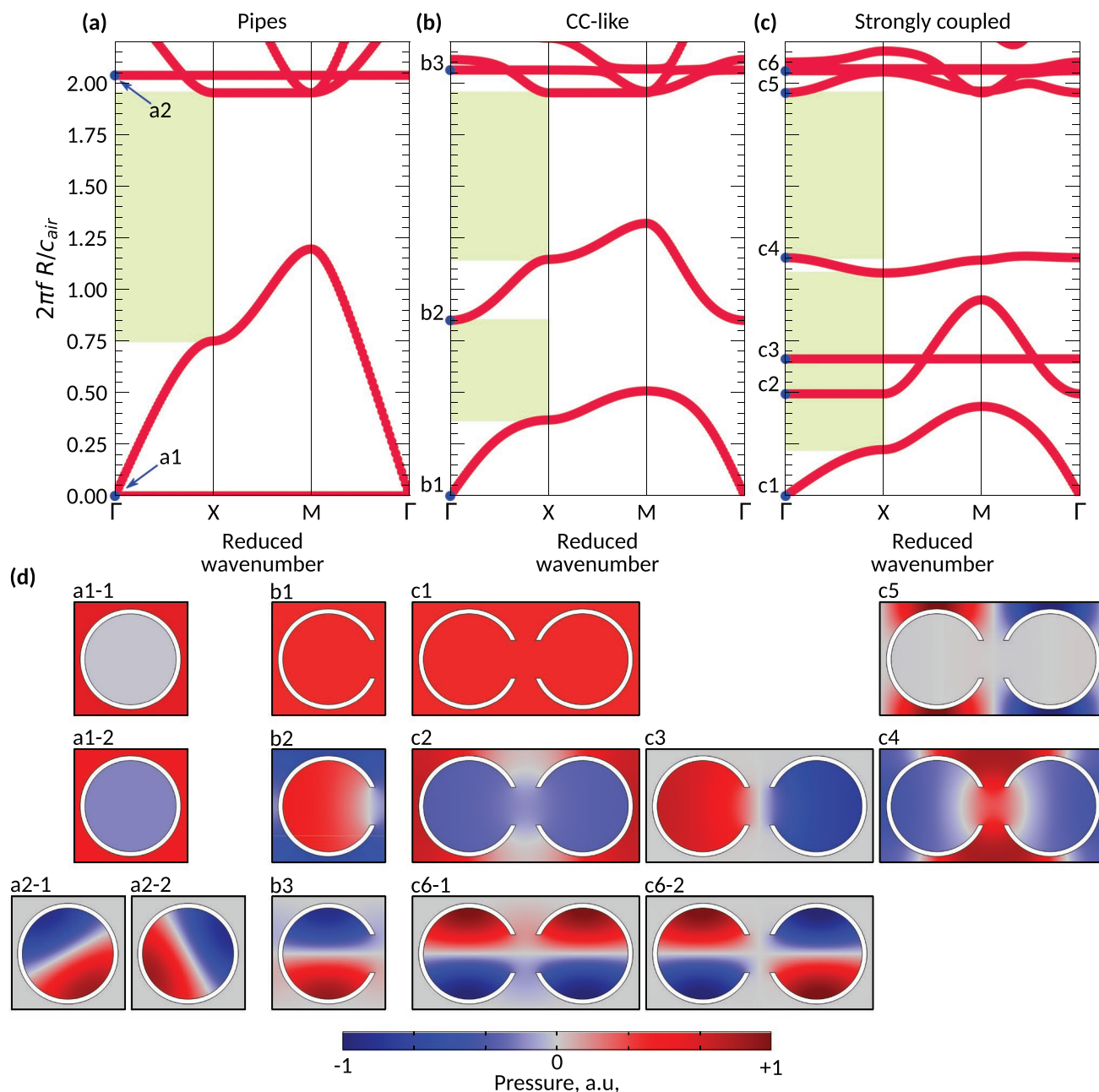TECHNOLOGIES
www.advmattechnol.de

Figure 5. Coupling between two resonators. The system consists of a pair of the Helmholtz resonators located in free space, such that the incident pressure field propagates along the x-axis. Two cases are considered, namely a) the CC-like geometry and d) the strongly coupled resonators. b,e) The corresponding frequency spectra calculated at the sampling point located at the center of the rightmost resonator (the red dot). The spectral distances between the split resonances for the case of interest $d/R = 2.25$ are indicated by Δ. c,f) Distributions of the scattered pressure field for the case of $d/R = 2.25$ are shown; the frequencies correspond to the resonances indicated by the vertical dashed lines on the spectra.

the outer radius of the resonators is $R = 53$ mm and the inner radius is $r = 48$ mm. Slit width is then $w = 40$ mm and the distance between the resonators is $d = 120$ mm. The considered frequency range is 200–2060 Hz.

The obtained transmission spectra are demonstrated in Figure 7e–g, where the blue lines correspond to 2D numerical simulations and the red lines represent the experimental measurements. The green shaded areas indicate the ΓX band-gaps of the equivalent infinite 2D system shown in Figure 7a. For convenience, two frequency axes are shown, the normalized (top) and the un-normalized (bottom). The measurements are

provided for 1, 2, and 3 pairs of resonators in order to explicitly demonstrate the evolution of stop-bands with respect to a change in the structure thickness. In accordance with intuition, increasing the number of pairs results in broadening of the stop-bands. It should be noted that, unlike the noise barrier consisting of a single Helmholtz resonator,[50] a wide stop-band can be observed even for the one-pair thickness. Practically, for the case of three pairs of coupled resonators, the stop-bands cover more than 80% of the considered spectral range. But even for one pair the stop-bands are quite large and pronounced, mostly going below the level of –15 dB.

**ADVANCED
SCIENCE NEWS**

www.advancedsciencenews.com

**ADVANCED
MATERIALS
TECHNOLOGIES**

www.advmattechnol.de

Figure 6. Evolution of the band structure. Band diagrams for the case of a) pipes, b) CC-like geometry c) strongly coupled resonators. Shaded green areas indicate the Γ–X band-gaps. The following parameters of the structures are used: (b) $w/R = 0.75$; (c) $w/R = 0.75$, $d/R = 2.25$; for each panel $r/R = 0.905$. Field distributions shown in panel (d) correspond to the labeled blue points in the band diagrams.

2.4. Noise-Insulating Chamber

The finite-size prototype of the metahouse chamber is shown in **Figure 8**a. It is an axially symmetric structure consisting of 30 radially oriented arrays with three pairs of resonators each. The outer radius of the chamber is 300 mm and the inner one is 120 mm. The height of the structure is 60 mm. The resonators are characterized by $R = 6.7$ mm, $r = 6$ mm, and $w = 5$ mm. Along the arrays, the distance between centers of the resonators (in xy plane) is $d = 15$ mm. The obtained transmission spectra are shown in Figure 8c with experimental values indicated by the red line and the 2D numerical simulations by the blue one. A schematic of the numerical model as well as additional calculations are presented in the Supporting Information. Shaded green areas indicate ΓX band-gaps of the corresponding infinite 2D system considered in the previous section. However, it should be noted that contrary to the previous case the unit cells of the chamber are not rectangular. The calculations presented in the Supporting Information demonstrate that tapering results in the increase
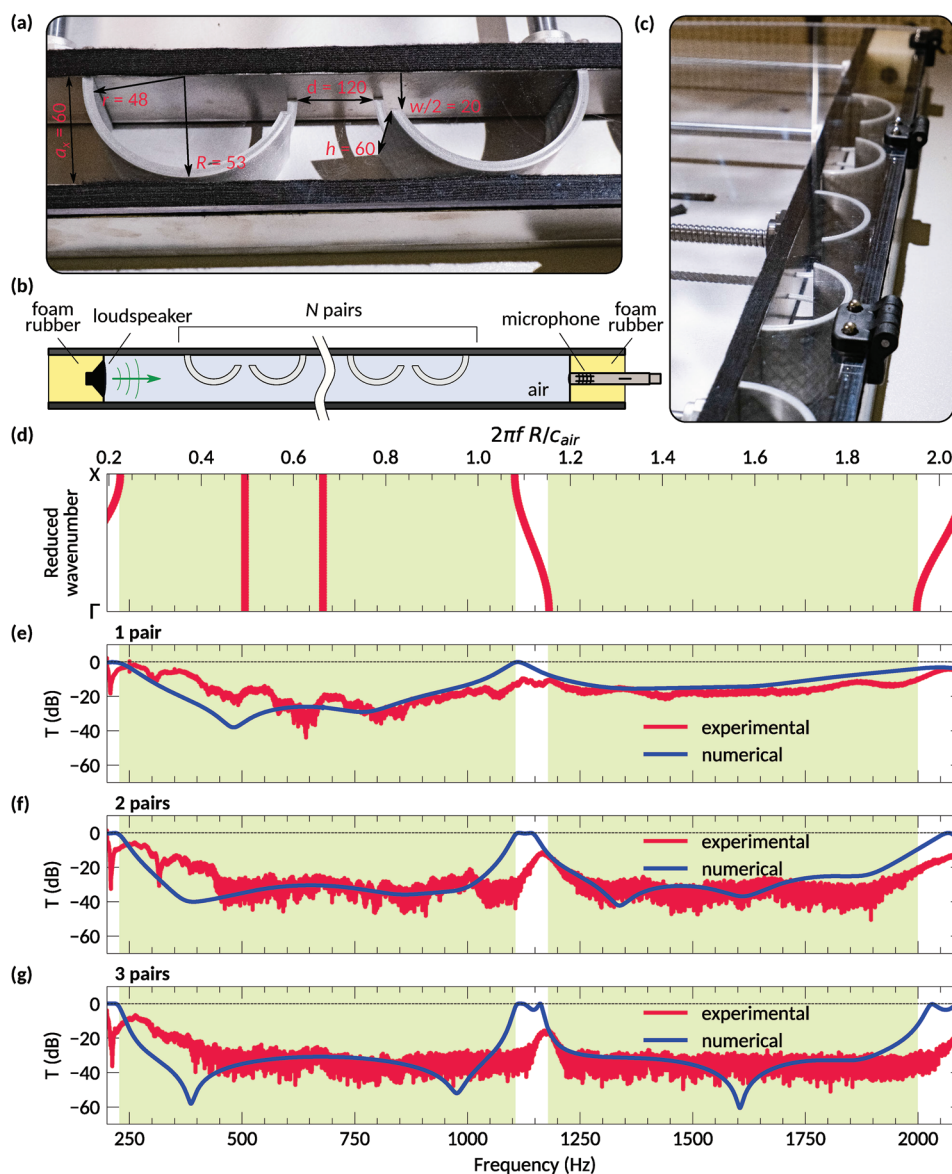
Figure 7. Transmission of semi-infinite structure. a) Photograph of the samples characterized by $R = 53$ mm, $r = 48$ mm, $w = 40$ mm, and height $h = 60$ mm. b) Schematic picture and c) photo of the experimental setup. d) Band diagram for the system with the unit cell with $a_x = 240$ mm, $a_y = 120$ mm, and $d = 120$ mm. For convenience, two frequency axes are shown, the normalized one and the one in conventional units. Measured and simulated (for a 2D system) transmission spectra for e) one, f) two, and g) three pairs of coupled Helmholtz resonators. Experimentally obtained values are shown by red lines, while the numerical results are given by the blue lines. Green shaded areas indicate ΓX band-gaps of the corresponding infinite 2D structure.

of the transmission coefficient, but it can still remain below −15 dB spectral average.

The measurements were performed in a box with walls covered by foam rubber pyramids (see Figure 8b). The height of the box is 60 mm while the wavelength of generated waves is smaller than this value for most of the considered frequency range (see Experimental Section). However, since all structures are uniform in the vertical direction, it is unlikely that the higher order modes would be excited. Due to the small size of the elements, it is quite difficult to avoid small gaps between the lid and the resonators which also may contradict the assumption that the structure is effectively infinite along the

axes of the resonators. However, the major differences between the results most probably originate from the low accuracy of 3D printing which is about 0.1–0.2 mm or 10–20% of the geometric scale of the structure. Hence, the experimental structure and the modeled one are not fully equivalent. Still, we assume that the fabrication accuracy is good enough to demonstrate the concept. We also would like to mention that presence of narrow bands with high transmission might be related to the change of the source radiated power also discussed in literature.[57,58] However despite these peaks the averaged noise suppression is large and the set of frequencies for which the suppression is achieved constitutes the major part of the spectra.
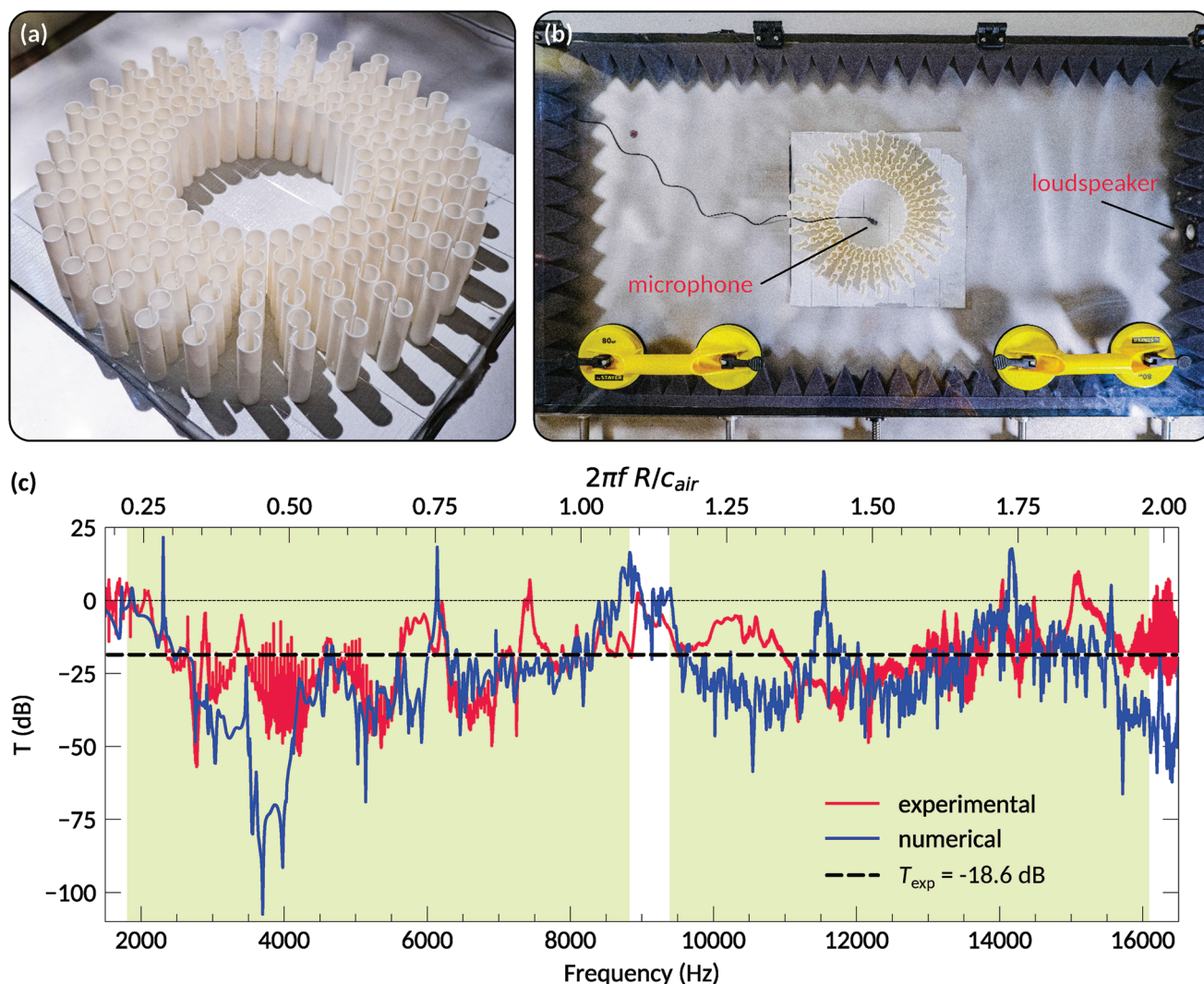
Figure 8. Transmission of the metahouse chamber. a) The manufactured prototype of the metahouse chamber. There are 30 arrays forming a toroid with the outer radius 300 mm and the inner one 120 mm. Each array consists of three pairs of resonators with $R = 6.7$ mm, $r = 5.5$ mm, and $w = 5$ mm. The distance between centers of the resonators along the axis of an array is $d = 15$ mm. b) Photograph of the experimental setup. The microphone is located inside the chamber and the loudspeaker is placed at one of the walls. c) Measured transmission spectrum (red line) and the corresponding numerical values obtained for the equivalent 2D chamber (blue line). Shaded green areas correspond to the equivalent infinite 2D periodic structure (see Figure 3).

3. Discussion

The developed metahouse chamber demonstrates good insulating properties with the average transmission of −18.6 dB in the broad spectral range from 1500 to 16500 Hz (Figure 8c). The average value was calculated as the arithmetic mean within the spectral range. This noise-mitigation properties are achieved due to formation of multiple stop-bands associated with bandgaps of a metamaterial and phononic crystal as for various wavelength the structure demonstrate different properties. Ventilation properties as well as partial optical transparency are defined by geometric parameters of the structure. Analysis of the air flow and optical transparency are presented in the Supporting Information. In **Table 1** we compare the presented structure with similar structures presented in the literature in order to demonstrate the advantages and disadvantages of the

proposed design. The main feature of the proposed structure is its multiple band noise suppression range together with possibility to achieve ventilation. At the same time, the structure has quite large geometric size. This is the consequence of the desired sparseness and the lack of proper optimization which may allow reducing the thickness of the chamber walls. Still, we should highlight once again that the goal of the present work was to achieve the largest range of noise mitigation together with the sparseness. Hence, there are no aims to solve a fundamental problem in acoustics requiring ultra-thin structures blocking low-frequency waves. However, considering a semi-infinite structure with a single pair of resonators, there is a pronounced attenuation in between 300 and 1100 Hz. In this case the thickness of the structure varies from 0.2λ to 0.8λ, meaning that the structure may have subwavelength thickness at low-frequency range and due to the scalability it can be

**ADVANCED
SCIENCE NEWS**

www.advancedsciencenews.com

**ADVANCED
MATERIALS
TECHNOLOGIES**

www.advmattechnol.de

Table 1. Comparison of the metahouse chamber with the similar types of noise-insulating structures.

Reference	Structure type	Noise suppression range, Hz	Thickness/length, mm	Passing airflow, %
This paper	Chamber	1500–16500	180 (single wall)	10–100
[49]	Chamber	2200–2600	65 (single wall)	40
[59]	Sparse array	1800–2600	31	100
[50]	Chamber	100–2900	38	not specified
[60]	Window	300–900	100–150	62–82
[61]	Window	250–2000	44	34
[62]	Duct	660–1200	96 (4 periods)	ventilated area 17–45%
[63]	Chamber	630–2000	25.4 (one wall)	not specified
[64]	Metamaterial	860–8000	110	not ventilated
[65]	Panel metamaterial	380–3600	72	not ventilated
[66]	Metasurface	600–2600	68	not ventilated

adjusted to specific frequencies. While thinner structures we presented in literature, for instance in refs. [38,51,53], the thickness of the proposed structure might be decreased with some optimization, which however is out the scope of this work.

While the concept was demonstrated for the case when the resonators are located quite close to each other, the structure may be optimized to increase the sparseness. For example, numerical calculations done for the finite-size metacage with the number of arrays reduced by a half also demonstrates reasonable noise-insulation properties with the average transmission being −7 dB (see Supporting Information). Tuning of parameters and optimization of the structure may enhance the results allowing increased air flow and optical transparency, implying a compromise between sparseness and sound transmission. In addition, the structure can be made from optically transparent materials, such as the commercially available PLA filament for 3D printers.[67] The possibility to achieve simultaneous air ventilation with optical transparency is a feature of the developed structure resulting from the proposed design. In **Table 2** we also provide values of acoustic impedance for several materials which may be used for construction of the metahouse chamber. It is important to highlight that the range of possible materials is huge and hence conventional, widely available materials can be used. Finally, it should be noted that we intentionally utilize an intuitive step-by-step approach, allowing a simple analysis of the physics behind the concept. In order to find a design with better performance an optimization techniques should be implemented, however that lies beyond the scope of this work. In addition, since the fabrication accuracy in our case is rather low optimization will not necessarily lead to a better experimental performance requiring more accurate reproduction of the geometric parameters.

Table 2. Acoustic impedance Z of some materials which can be used for construction of the metahouse chamber.

Material	Z (MRayl)	Reference
Polylactic acid (PLA)	2.56–2.77	[68]
Polypropylene	2.3–2.4	[69]
Polymethyl methacrylat	3.14–3.69	[70]

4. Experimental Section

Numerical Simulations: All numerical simulations were performed for 2D systems using the finite element method via COMSOL multiphysics, pressure acoustics module. Throughout the calculations, the boundaries of the resonators were assumed to be sound-hard walls. Such an approximation was justified by the high impedance contrast between the material of the resonators and air. For example, the acoustic impedance of polypropylene was about 2.4 MRayl[69] which was six orders higher than for air. Similar contrast of impedance was also observed for other materials which can be used for construction of the chamber, see Table 2. Thermo-viscous boundary effects were neglected in the simulation, since they were only significant in the presence of narrow channels, which were not present in the considered structures.

The semi-infinite structure was modeled as an array made from N halved resonators placed into a 2D waveguide with sound hard walls. The distance between the walls was equal to $a_y/2$. The ends of the waveguide were modeled as perfectly matched layers (PML). The incident plane wave with amplitude p_0 propagated along the direction of periodicity (x-axis, parallel to the walls of the waveguide). Pressure values were calculated at the sample point located at the distance $x_t = 15$ mm from the right-most resonator. The geometric parameters of the resonators corresponded to those of the fabricated samples.

In the model for the finite-size case the chamber was placed into the 2D box in which all walls were PML such that the distance between the walls was 1210 and 510 mm along x and y axis, respectively. The structure was located at the center of the waveguide and the sample point was placed at the center of the structure. Incident waves with amplitude p_0 were generated by a point source located near one of the walls. The size of the 2D chamber corresponded to the parameters of the manufactured structure.

Experimental Setup: The experimental measurements were performed inside a waveguide with rectangular cross-section. The walls and the bottom of the waveguide were made of aluminum with thickness of 15 mm. The lid was made of 6 mm thick transparent plexiglass. The height of the inner cross-section of the waveguide was fixed and equal to 60 mm. However, the width was adjustable and can be varied from 0 to 650 mm via displacement of one of the walls. The loudspeaker (Visaton BF 45/4) was located at one end of the waveguide and the microphone (BOYA BY-PVM1000) was placed at the other end. While the full length of the waveguide was 135 cm, the distance between the microphone and the loudspeaker was 107 cm. The rest of the waveguide's length was occupied by two pieces of foam rubber, each 14 cm long. The loudspeaker and the microphone were embedded into these inserts.

**ADVANCED
SCIENCE NEWS**
www.advancedsciencenews.com

**ADVANCED
MATERIALS
TECHNOLOGIES**
www.advmattechnol.de

The microphone was directly connected to a USB audio interface Roland Rubix22. To connect the loudspeaker to the same sound card an amplifier based on the Yamaha YDA138-E microchip was used. The sound card was connected to a personal computer via USB interface. Control of signal generation and recording was realized via specially developed software based on the Python programming language (in particular, generation and recording of signals exploit the sound device module[71]).

To imitate a semi-infinite structure in the experiment an array consisting of N pairs of coupled resonators were considered. Proper boundary conditions—namely, sound hard walls at geometrical symmetry axes—imitated periodicity along the two other axes (y and z axes). The 2D numerical model corresponded to a structure infinite in the z direction, while in the experiment it was mimicked by keeping the waveguide width and height smaller than $\lambda/2$ for the considered spectral range. The operational frequency range of the setup for the semi-infinite structure was 200–2100 Hz. The size of the cross-section was selected such that its width and height were smaller than the smallest wavelength in the spectrum of a generated signal, to preserve the symmetry of the unit cell and of field distributions within it. Otherwise, the walls would have to be perfectly symmetric and elements within the waveguide would have to be centered ideally, which are difficult to achieve. In order to increase the reliable frequency range in the waveguide below $\lambda/2$, half instead of full resonators were therefore used. Such modification was valid since it did not violate symmetry of the structure. The resonators were manufactured by 3D printing (PLA filament). Note, that to simplify placement of resonators inside the waveguide, there were small placeholders in the slits of the resonators.

All measurements were conducted with a chirped signal with the frequency swept from 200 to 2100 Hz. For each measurement the signal was generated several times and then the measured spectra were averaged in Fourier space. The sampling frequency was fixed at 44 100 Hz. Following the conventional definition, the transmission is defined as

$$T = 20 \log(p_{tr}/p_{ref}) \tag{2}$$

where p_{ref} is the reference pressure amplitude of the wave in the absence of the structure and p_{tr} is a pressure amplitude of the transmitted wave.

The transmission measurements for the finite-size chamber were conducted in the same waveguide, as the semi-infinite structure. However, the distance between the walls was increased to 650 mm. The walls and the ends were covered by foam rubber pyramids (with height 50 mm and square base 50 by 50 mm). The chamber was located at the center of the waveguide and a microphone (BOYA BY-M1) was placed at the center of the structure. All other elements and connections between them were the same as for the semi-infinite system. The procedure of signal generation and averaging also remained the same, however the frequency range was changed to 1500 to 16 500 Hz.

Supporting Information

Supporting Information is available from the Wiley Online Library or from the author.

Acknowledgements

Conflict of Interest

The authors declare no conflict of interest.

Author Contributions

M.K. designed the structure, experimental samples, and the experimental setup, and performed experimental measurements. S.K. and M.K. provided numerical calculations. S.K. participated in the experimental setup assembly and measurements. A.M., Y.B., S.M., and D.P. provided guidance on all aspects of the work. A.B. suggested the idea and supervised the project. All authors contributed to writing and editing of the manuscript.

Data Availability Statement

Research data are not shared.

Keywords

[1] S. A. Cummer, J. Christensen, A. Alù, *Nat. Rev. Mater.* **2016**, *1*, 16001.

[2] F. Zangeneh-Nejad, R. Fleury, *Rev. Phys.* **2019**, *4*, 100031.

[3] J. Liu, H. Guo, T. Wang, *Crystals* **2020**, *10*, 305.

[4] G. Liao, C. Luan, Z. Wang, J. Liu, X. Yao, J. Fu, *Adv. Mater. Technol.* **2021**, *6*, 2000787.

[5] N. Kaina, F. Lemoult, M. Fink, G. Lerosey, *Nature* **2015**, *525*, 77.

[6] J. de Rosny, M. Fink, *Phys. Rev. Lett.* **2002**, *89*, 124301.

[7] J. Li, L. Fok, X. Yin, G. Bartal, X. Zhang, *Nat. Mater.* **2009**, *8*, 931.

[8] J. Zhang, Y. Tian, Y. Cheng, X. Liu, *Appl. Phys. Lett.* **2020**, *116*, 030501.

[9] H. Chen, C. T. Chan, *Appl. Phys. Lett.* **2007**, *91*, 183518.

[10] X. Guo, Y. Ding, Y. Duan, X. Ni, *Light: Sci. Appl.* **2019**, *8*, 123.

[11] Y.-G. Peng, C.-Z. Qin, D.-G. Zhao, Y.-X. Shen, X.-Y. Xu, M. Bao, H. Jia, X.-F. Zhu, *Nat. Commun.* **2016**, *7*, 13368.

[12] H. Xue, Y. Ge, H.-X. Sun, Q. Wang, D. Jia, Y.-J. Guan, S.-Q. Yuan, Y. Chong, B. Zhang, *Nat. Commun.* **2020**, *11*, 2442.

[13] X. Fang, J. Wen, B. Bonello, J. Yin, D. Yu, *Nat. Commun.* **2017**, *8*, 1288.

[14] S. Chen, Y. Fan, Q. Fu, H. Wu, Y. Jin, J. Zheng, F. Zhang, *Appl. Sci.* **2018**, *8*, 1480.

[15] B. Xie, K. Tang, H. Cheng, Z. Liu, S. Chen, J. Tian, *Adv. Mater.* **2017**, *29*, 1603507.

[16] Z. Tian, C. Shen, J. Li, E. Reit, Y. Gu, H. Fu, S. A. Cummer, T. J. Huang, *Adv. Funct. Mater.* **2019**, *29*, 1808489.

[17] S. Zuo, Q. Wei, Y. Tian, Y. Cheng, X. Liu, *Sci. Rep.* **2018**, *8*, 10103.

[18] K. Donda, Y. Zhu, A. Merkel, S.-W. Fan, L. Cao, S. Wan, B. Assouar, *Smart Mater. Struct.* **2021**.

[19] Z.-X. Xu, B. Zheng, J. Yang, B. Liang, J.-C. Cheng, *Phys. Rev. Appl.* **2021**, *16*, 044020.

[20] N. Gao, M. Wang, B. Cheng, H. Hou, *Appl. Acoust.* **2021**, *180*, 108153.

[21] H. Ding, X. Fang, B. Jia, N. Wang, Q. Cheng, Y. Li, *Phys. Rev. Appl.* **2021**, *16*, 064035.

[22] W. Zhou, Y. Su, Muhammad, W. Chen, C. W. Lim, *Int. J. Mech. Sci.* **2020**, *172*, 105368.

[23] X.-D. Fan, L. Zhang, *Phys. Rev. Res.* **2021**, *3*, 013251.

[24] C. Shi, R. Zhao, Y. Long, S. Yang, Y. Wang, H. Chen, J. Ren, X. Zhang, *Natl. Sci. Rev.* **2019**, *6*, 707.

[25] Y. Long, D. Zhang, C. Yang, J. Ge, H. Chen, J. Ren, *Nat. Commun.* **2020**, *11*, 4716.

[26] C. Yang, Y.-T. Tan, H. Chen, J. Ren, *J. Appl. Phys.* **2021**, *129*, 135106.

[27] S. Wang, G. Zhang, X. Wang, Q. Tong, J. Li, G. Ma, *Nat. Commun.* **2021**, *12*, 6125.

[28] H. Ge, X.-Y. Xu, L. Liu, R. Xu, Z.-K. Lin, S.-Y. Yu, M. Bao, J.-H. Jiang, M.-H. Lu, Y.-F. Chen, *Phys. Rev. Lett.* **2021**, *127*, 144502.

[29] S. M. Gardezi, H. Pirie, S. Carr, W. Dorrell, J. E. Hoffman, *2D Mater.* **2021**, *8*, 031002.

[30] N. Gao, Z. Zhang, J. Deng, X. Guo, B. Cheng, H. Hou, *Adv. Mater. Technol.* **2022**, *7*, 2100698.

[31] S. A. Stansfeld, M. P. Matheson, *Br. Med. Bull.* **2003**, *68*, 243.

[32] N. Singh, S. C. Davar, *J. Human Ecol.* **2004**, *16*, 181.

[33] L. Goines, L. Hagler, *South. Med. J.* **2007**, *100*, 287.

[34] H. P. Kunc, R. Schmidt, *Biol. Lett.* **2019**, *15*, 20190649.

[35] T. Münzel, M. Sørensen, A. Daiber, *Nat. Rev. Cardiol.* **2021**, *18*, 619.

[36] C. Hopkins, *Sound Insulation*, Routledge, London **2007**.

[37] Z.-X. Xu, H. Gao, Y.-J. Ding, J. Yang, B. Liang, J.-C. Cheng, *Phys. Rev. Appl.* **2020**, *14*, 054016.

[38] M. Sun, X. Fang, D. Mao, X. Wang, Y. Li, *Phys. Rev. Appl.* **2020**, *13*, 044028.

[39] S. Kumar, T. B. Xiang, H. P. Lee, *Appl. Acoust.* **2020**, *159*, 107088.

[40] R. Dong, D. Mao, X. Wang, Y. Li, *Phys. Rev. Appl.* **2021**, *15*, 024044.

[41] R. Dong, M. Sun, F. Mo, D. Mao, X. Wang, Y. Li, *54*, 403002.

[42] G. Ma, M. Yang, Z. Yang, P. Sheng, *Appl. Phys. Lett.* **2013**, *103*, 011903.

[43] F. Langfeldt, H. Kemsies, W. Gleine, O. von Estorff, *Phys. Lett. A* **2017**, *381*, 1457.

[44] Y. Cheng, C. Zhou, B.-G. Yuan, D.-J. Wu, Q. Wei, X.-J. Liu, *Nat. Mater.* **2015**, *14*, 1013.

[45] Z. Chen, L. Fan, S.-Y. Zhang, H. Zhang, X.-J. Li, J. Ding, *Appl. Phys. Express* **2015**, *8*, 107301.

[46] H.-L. Zhang, Y.-F. Zhu, B. Liang, J. Yang, J. Yang, J.-C. Cheng, *Appl. Phys. Lett.* **2017**, *111*, 203502.

[47] R. Ghaffarivardavagh, J. Nikolajczyk, S. Anderson, X. Zhang, *Phys. Rev. B* **2019**, *99*, 024302.

[48] X. Yu, Z. Lu, T. Liu, L. Cheng, J. Zhu, F. Cui, *J. Sound Vib.* **2019**, *449*, 140.

[49] C. Shen, Y. Xie, J. Li, S. A. Cummer, Y. Jing, *J. Appl. Phys.* **2018**, *123*, 124501.

[50] A. Melnikov, M. Maeder, N. Friedrich, Y. Pozhanka, A. Wollmann, M. Scheffler, S. Oberst, D. Powell, S. Marburg, *J. Acoustical Soc. Am.* **2020**, *147*, 1491.

[51] C. Liu, J. Shi, W. Zhao, X. Zhou, C. Ma, R. Peng, M. Wang, Z. H. Hang, X. Liu, J. Christensen, N. X. Fang, Y. Lai, *Phys. Rev. Lett.* **2021**, *127*, 084301.

[52] X. Wang, X. Luo, B. Yang, Z. Huang, *Appl. Phys. Lett.* **2019**, *115*, 171902.

[53] J. Carbajo, S. Ghaffari Mosanenzadeh, S. Kim, N. X. Fang, *Appl. Phys. Lett.* **2020**, *116*, 054101.

[54] A. Melnikov, Y. K. Chiang, L. Quan, S. Oberst, A. Alù, D. Powell, S. Marburg, *Nat. Commun.* **2019**, *10*, 3148.

[55] D. P. Elford, L. Chalmers, F. V. Kusmartsev, G. M. Swallowe, *J. Acoust. Soc. Am.* **2011**, *130*, 2746.

[56] G. Hu, L. Tang, R. Das, S. Gao, H. Liu, *AIP Adv.* **2017**, *7*, 025211.

[57] P. M. Morse, K. U. Ingard, *Theoretical Acoustics*, Princeton University Press, Princeton **1986**.

[58] L. E. Kinsler, A. R. Frey, A. B. Coppens, J. V. Sanders, *Fundamentals of Acoustics*, 4th ed., Wiley, New York **2000**.

[59] T. Lee, T. Nomura, E. M. Dede, H. Iizuka, *Phys. Rev. Appl.* **2019**, *11*, 024022.

[60] X. Xiang, X. Wu, X. Li, P. Wu, H. He, Q. Mu, S. Wang, Y. Huang, W. Wen, *Extreme Mech. Lett.* **2020**, *39*, 100786.

[61] R. Dong, D. Mao, X. Wang, Y. Li, *Phys. Rev. Appl.* **2021**, *15*, 024044.

[62] Z. Xiao, P. Gao, D. Wang, X. He, L. Wu, *Extreme Mech. Lett.* **2021**, *46*, 101348.

[63] S. Kumar, J. W. Aow, H. P. Lee, *Appl. Acoust.* **2022**, *193*, 108779.

[64] L. Liu, L.-X. Xie, W. Huang, X. J. Zhang, M.-H. Lu, Y.-F. Chen, *Appl. Phys. Lett.* **2022**, *120*, 251701.

[65] C. Rui Liu, J. Hui Wu, Z. Yang, F. Ma, *Compos. Struct.* **2020**, *246*, 112366.

[66] Y. Zhu, A. Merkel, K. Donda, S. Fan, L. Cao, B. Assouar, *Phys. Rev. B* **2021**, *103*, 064102.

[67] B. D. M. Matos, V. Rocha, E. J. da Silva, F. H. Moro, A. C. Bottene, C. A. Ribeiro, D. dos Santos Dias, S. G. Antonio, A. C. do Amaral, S. A. Cruz, H. G. de Oliveira Barud, H. da Silva Barud, *J. Therm. Anal. Calorim.* **2019**, *137*, 555.

[68] N. G. Parker, M. L. Mather, S. P. Morgan, M. J. W. Povey, *Biomed. Mater.* **2010**, *5*, 055004.

[69] A. R. Selfridge, *IEEE Trans. Son. Ultrason.* **1985**, *32*, 381.

[70] J. E. Carlson, J. van Deventer, A. Scolan, C. Carlander, in *IEEE Symp. on Ultrasonics*, Vol. *1*, IEEE, Piscataway, NJ **2003**, pp. 885–888.

[71] Play and Record Sound with Python—python-sounddevice, https://python-sounddevice.readthedocs.io (accessed: July 2022).